Continuous magnetic phase transition in half-frustrated $Ca_2Os_2O_7$

P. Zheng,[1] Y. G. Shi,[1] Q. S. Wu,[1] G. Xu,[1] T. Dong,[1] Z. G. Chen,[1] R. H. Yuan,[1] B. Cheng,[1] K. Yamaura,[2] J. L. Luo,[1] and N. L. Wang[1]

[1]*Beijing National Laboratory for Condensed Matter Physics, Institute of Physics, Chinese Academy of Sciences, Beijing 100080, People's Republic of China*

[2]*Superconducting Properties Unit, National Institute for Materials Science, 1-1 Namiki, Tsukuba, 305-0044 Ibaraki, Japan*

(Received 27 August 2012; published 7 November 2012)

We present the specific heat, magnetization, optical spectroscopy measurements, and the first-principles calculations on the Weberite structure $Ca_2Os_2O_7$ single-crystal/polycrystalline sample. The $Ca_2Os_2O_7$ shows a Curie-Weiss nature at high temperature and goes into a ferrimagnetic insulating state at 327 K on cooling. A λ-like peak is observed at 327 K in the specific heat implying a second-order phase transition. The vanishing electronic specific heat at low temperature suggests a full energy gap. At high temperature above the transition, a small amount of itinerant carriers with short life time τ is observed, which is gapped at 20 K with a direct gap of 0.24 eV. Our first-principles calculations indicate that the antiferromagnetic (AFM) correlation with intermediate Coulomb repulsion U could effectively split Os(4*b*) t_{2g} bands and push them away from Fermi level (E_F). On the other hand, a noncollinear magnetic interaction is needed to push the Os(4*c*) bands away from E_F, which could be induced by Os(4*c*)-Os(4*c*) frustration. Therefore, AFM correlation, Coulomb repulsion U and noncollinear interaction all play important roles for the insulating ground state in $Ca_2Os_2O_7$.

DOI: 10.1103/PhysRevB.86.195108 PACS number(s): 71.30.+h, 72.80.Ga, 78.30.−j

I. INTRODUCTION

Metal-insulator transition (MIT) is one of the important phenomena in condensed matter physics and has attracted much attention. Many transition-metal oxides containing partially filled *d* orbitals, such as NiO, V_2O_3, have been identified experiencing such transition.[1–3] Mott and Hubbard proposed that the on-site Coulomb interaction plays an important role in the narrow band materials.[4] Large on-site Coulomb repulsion energy could split the band into two. In general, the correlation effect depends on the value of U/W, where W is the band width, and U is the Coulomb repulsion energy. For 3*d* transition metal oxides, the band width W is small and the Coulomb repulsion energy (U) is relatively big, which could lead to $U/W \gg 1$. So 3*d* metal oxides usually belong to strong correlation limit and many of them would be insulating. For 4*d*/5*d* metal oxides,[5] their band widths W are larger than that of 3*d* compounds. The larger spatial extent of 4*d*/5*d* wave functions also means that the on-site Coulomb repulsion is smaller. Therefore 4*d*/5*d* materials are generally less strongly correlated than 3*d* materials, and lead to $U/W \sim 1$. Simultaneously, as the atomic mass increases, the spin-orbital coupling (SOC) becomes more and more important, which also plays an essential role in 4*d*/5*d* materials. With these two effects, the electronic properties of 4*d*/5*d* metal oxides become more complex and abundant; many new physical phenomena emerge.

Recently, some partially filled 5*d* transition metal oxides, such as Sr_2IrO_4,[6,7] $Cd_2Os_2O_7$,[8] $Ca_2Os_2O_7$,[9] Ca_3LiOsO_6,[10] etc., were found insulating at low temperature, which stimulated many experimental and theoretical studies.[6–9,11] One novel type of Mott insulating state was observed in the Ir^{+4}-based Sr_2IrO_4.[7] The unusual insulating state is attributed to the cooperative interactions of electron correlation and large spin-orbital coupling.[6] This study is very helpful to the understanding of the MIT in 5*d* transition metal compounds. On the other hand, for the pyrochlore structure material $Cd_2Os_2O_7$, a continuous metal-insulator transition was observed by resistance, specific heat, magnetization, Hall effect, thermal conductivity, and the optical conductivity measurements.[8,11] In this compound, Os 5*d* t_{2g} bands are half filled because that the $Cd_2Os_2O_7$ adopts the octahedral environment of OsO_6 with $5d^3$ configuration so that the t_{2g} band is expected near half filling. As we all know, SOC is weak in $S = 3/2$ configuration of the half-filled t_{2g} band for its total orbital angular momentum $L = 0$. One more important issue in $Cd_2Os_2O_7$ is that every Os ion is shared by two Os tetrahedrons, and frustrated with each other. The large nearest-neighbor coordination number would cause a wider Os band width.[12] So the mechanism proposed in Sr_2IrO_4 is not suitable for $Cd_2Os_2O_7$. Padilla *et al.* attributed this continuous metal-insulator transition in $Cd_2Os_2O_7$ to a Slater transition,[8] which is driven by the AFM correlation. The K_4CdCl_6 type Ca_3LiOsO_6 is another Os^{5+} oxide with the $5d^3$ electronic configuration, in which the t_{2g} orbitals are half-filled with $S = 3/2$. Similarly, the SOC is weak in this case, and it is not surprising that the calculation with LDA + SOC can not split the Os $5dt_{2g}$ bands into two manifolds.[10] However, comparing with $Cd_2Os_2O_7$, half the Os atoms are replaced by Li atoms in Ca_3LiOsO_6. The nearest-neighbor Os atoms are rather distant, and the magnetic interaction is expected to be rather weak, regardless of the structural anisotropy. Therefore, the magnetic frustration is almost quenched. Band structure calculation shows that the bandwidth of t_{2g} bands is narrower than for other typical Os oxides. The smaller bandwidth is a direct consequence of the local structure around Os atoms.[10] The narrow t_{2g} bands suggest that correlation effects are important for this compound, although the Coulomb interaction is expected to be weak due to the nature of the 5*d* orbital. Shi *et al.* claim that Ca_3LiOsO_6 can be considered as a 5*d* Mott insulator, which stabilized within a collinear AFM (antiparallel) phase.[10]

$Ca_2Os_2O_7$ is another Os^{+5} oxide with the $5d^3$ electronic configuration but adopts the Weberite structure[9] (see Fig. 1). In this structure, Ca cations have two different coordinations

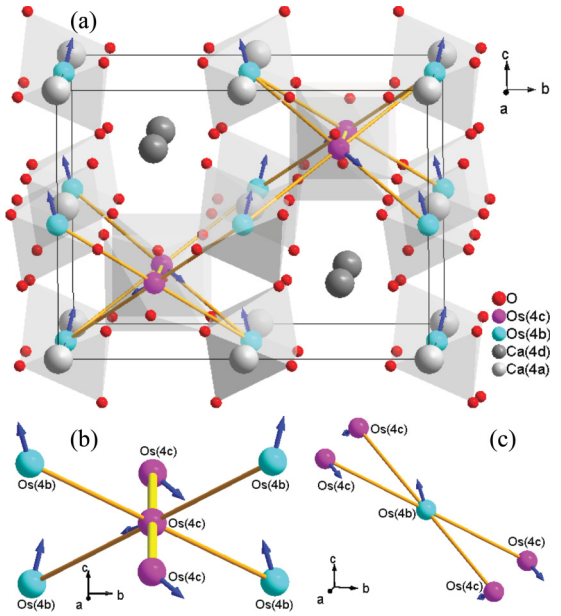

FIG. 1. (Color online) (a) The crystal structure of $Ca_2Os_2O_7$, with the 4*a* site Ca^{2+} on (0, 0, 0), the 4*d* site Ca^{2+} on (1/4, 1/4, 3/4), the 4*c* site Os^{5+} on (1/4, 1/4, 1/4), and the 4*b* site Os^{5+} on (0, 0, 1/2) in the crystal. (b) Coordination environments of Os(4*c*) in $Ca_2Os_2O_7$. (c) Coordination environments of Os(4*b*) in $Ca_2Os_2O_7$. A dark blue arrow represents a spin director of Os ion. The orange bonds connect the nearest-neighboring Os(4*b*) and Os(4*c*) ions. The yellow bonds connect the nearest-neighboring Os(4*c*) and Os(4*c*) ions.

(4*a* and 4*d*) with eight oxygen ions. Each Os^{5+} is octahedrally coordinated by six nearest oxygen atoms. There are two different Os cation environments. One is the Os(4*b*) site, which coordinates with four unfrustrated nearest-neighboring Os(4*c*) cations. The other one is the Os(4*c*) site, which has six nearest-neighboring Os cations. Beside four unfrustrated Os(4*b*) cations, it is also coordinated by two frustrated Os(4*c*) cations. So we name $Ca_2Os_2O_7$ as the half-frustrated system. The frustration effect would lead to a noncollinear magnetic interaction.[12] Up to now, only the temperature dependencies of resistivity and crystal structure on polycrystal were reported. Similar to $Cd_2Os_2O_7$, $Ca_2Os_2O_7$ also has an insulating ground state[9] and shows a metal-insulator-like transition. However, its magnetic properties, electronic structure and the origin of the M-I transition are not studied yet. In this work, we present investigations on $Ca_2Os_2O_7$ by the resistance, specific heat, magnetization, and optical reflectance measurements. The resistivity reproduces the behavior reported in Ref. 9, which also shows an insulating state at low temperature. Zero electronic specific heat is observed, implying a full gap at the low temperature. In the meantime, a spectral weight transferring from low frequency to high frequency in optical conductivity is observed with decreasing temperature, conforming the gap opening in the insulating state. A high-temperature magnetization study indicates that the system is stabilized in high spin state with $S = 3/2$. To explain the experimental observations, the first-principles calculations are performed. We find that the AFM correlation with intermediate Coulomb repulsion U plays an important role during Os(4*b*) bands splitting. But for Os(4*c*) bands, the noncollinear magnetic interaction is another necessary factor.

II. EXPERIMENT

High-density polycrystal and small single-crystal samples were prepared in a high-pressure apparatus. The stoichiometric mixtures of CaO, OsO_2 (Os-84.0%, Alfa Aesar), and $KClO_4$ were placed into a platinum capsule and sintered in a belt-type high-pressure apparatus at 1300 °C for one hour under a pressure of 3 GPa. We washed the polycrystal to remove the KCl flux. The powder samples were pressed again at 6 GPa to get the condensed pellets, which were used for measuring the specific heat, resistivity, and optical reflectance data. The single crystal grew under a stable pressure of 3 GPa during heating at 1500 °C for two hours (KCl as flux provided by $KClO_4$), then was slowly cooled down to 1300 °C for three hours. Thereafter, the capsule was quenched to ambient pressure and temperature. The samples were washed by water several times and we could find some single crystals. Typically, the crystals have square shape of surface with edge length of about 0.2 mm. The largest single crystal has an edge length of about 0.5 mm. X-ray diffraction measurement at room temperature indicates that the samples are of single phase with Weberite structure. The crystal structure and main interatomic distances are collected in Table I, which are very close to the previous report.[9] The dc resistivity [$\rho(T)$] and the specific heat (C_p) measurements were carried out on a quantum design physical property measurement system (PPMS). The magnetization was measured on a quantum design (SQUID) VSM. The optical reflectance $R(w)$ of $Ca_2Os_2O_7$ was measured from 30 cm^{-1} to 25 000 cm^{-1} at different temperatures on a Fourier transform spectrometer (Bruker 80v). Standard Kramers-Kronig transformations were employed to derive the frequency-dependent optical conductivity. For low-frequency extrapolations, we use Hagen-Rubens relation for the measurements above 300 K and constant values for reflectance data below 200 K. In fact, it is found that the different low-frequency extrapolations do not affect the conductivity spectra in the measured frequency region. On the high-energy side, the measured reflectance curve is extrapolated constantly to 100 000 cm^{-1}, above which a well-known function of ω^{-4} is used.

The electronic structures of $Ca_2Os_2O_7$ are studied by first-principles calculations using the BSTATE and VASP packages. Both of them are based on the plane-wave method

TABLE I. The parameters of the crystal structure and main interatomic distances at room temperature; group space: *Imma*; cell parameters: $a = 7.2165$ Å, $b = 10.1385$ Å, $c = 7.3844$ Å; Ca(4*a*) on (0, 0, 0), Ca(4*d*) on (1/4, 1/4, 3/4), Os (4*c*) on (1/4, 1/4, 1/4), Os (4*b*) on (0, 0, 1/2), O1 on (0, 1/4, 0.1625), O2 on (0, 0.4038, 0.7279); O3 on (0.2054, 0.3834, 0.4356).

Ca(4*a*)–O2	2.2335 Å
Ca(4*d*)–O2	2.3902 Å
Os(4*c*)–O1	1.9163 Å
Os(4*b*)–O2	1.9451 Å
Os(4*b*)–Os(4*c*)	3.6176 Å
Os(4*c*)–Os(4*c*)	3.6082 Å

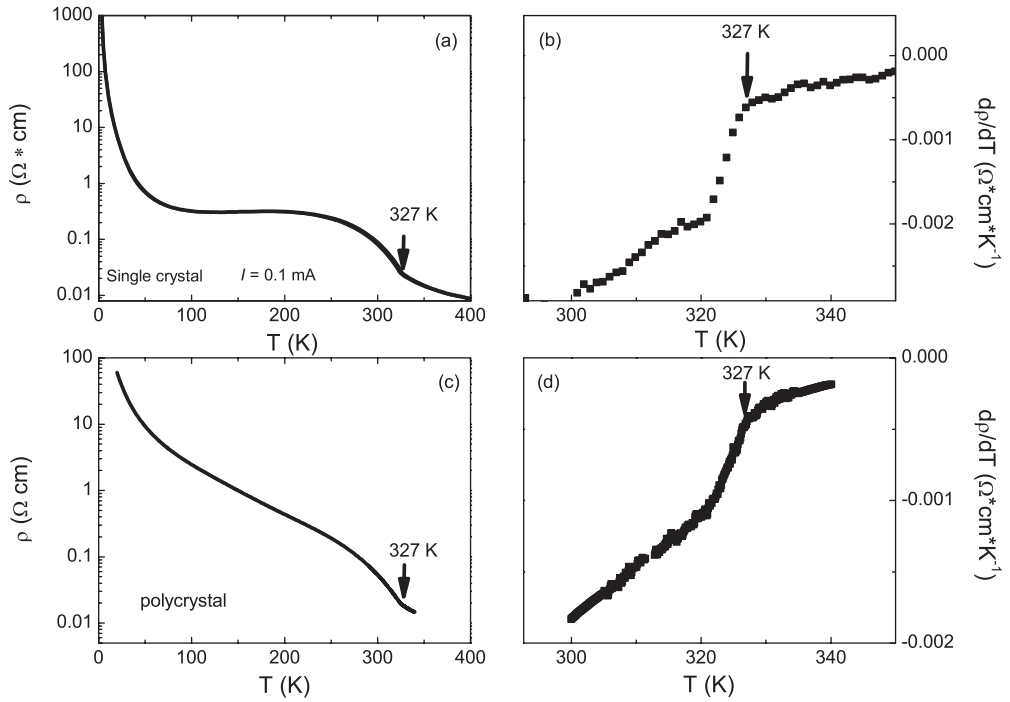

FIG. 2. (a)–(d) The temperature dependence of resistivity(ρ) and $d\rho/dT$ of $Ca_2Os_2O_7$ single crystal and polycrystalline sample respectively.

with pseudopotential scheme, and give consistent results. The generalized gradient approximation (GGA) of PBE-type[13] and its variant GGA + U method are used for the exchange-correlation energy. Nonmagnetic (NM), collinear antiferromagnetic (AFM), and noncollinear magnetic states are considered in the present study. All calculations are performed with the experimental lattice parameters and internal coordinates. Spin-orbital coupling (SOC) is considered in all calculations. However, as identified in other Os^{5+} compounds such as $Cd_2Os_2O_7$[14] and Ca_3LiOsO_6,[10] SOC plays very weak roles on the NM electronic structures and collinear magnetism.

The temperature-dependent dc resistivities [$\rho(T)$] for both single-crystal and polycrystalline samples are shown in Fig. 2. They show similar temperature dependence. A spinodal feature could be found in $\rho(T)$. The spinodals of the two samples appear at the same temperature [Figs. 2(a) and 2(c)]. The resistivity at 300 K is ten times higher than the value for $Cd_2Os_2O_7$[11] but one percent of the value for Ca_3LiOsO_6.[10] We calculate their $d\rho/dT$ [Figs. 2(b) and 2(d)] to determine the phase transition temperature. The sharp drop of $d\rho/dT$ begins at 327 K for both samples. $d\rho/dT$ of the single crystal changes more pronouncedly than that of the polycrystal. Both the XRD result and the $\rho(T)$ imply the high quality of our samples and that the polycrystalline sample is very close to the single crystal.

The magnetic properties of $Ca_2Os_2O_7$ under magnetic fields are shown in Figs. 3(a)–3(c). Figure 3(a) is the inverse susceptibility[$1/\chi(T)$] from 300 K to 550 K. An abrupt change occurs at the same critical temperature with the resistivity anomaly. The data between 320 K and 400 K deviate from the linear-T dependence. When temperature is higher than 400 K, $1/\chi$ shows a good linear relation with T, suggesting a paramagnetic Curie-Weiss behavior, $\chi = N\mu_0\mu_J^2/3k_B(T - \theta)$, from which we can estimate the system's intrinsic magnetic moment in terms of $C = N\mu_0\mu_J^2/3k_B$. Here θ is the Weiss temperature; N is the Avogadro's constant; k_B is the Boltzmann constant; $\mu_J = g\sqrt{S(S+1)}\,\mu_B$ (Lande factor $g = 2$) is the intrinsic magnetic moment. By fitting the data from 450 K to 550 K [shown in the inset of Fig. 3(a)], the intrinsic magnetic moment per Os ion is determined to be 2.59 μ_B. This value is about 67% of the expected moment (3.87 μ_B/Os) for $S = 3/2$ configuration, indicating that the spins of Os 5d electrons are in the $S = 3/2$ high spin state. θ is -1263 K, suggesting a strong antiferromagnetic interaction.

Figure 3(b) shows the temperature dependencies of the magnetization $M(T)$ measured with 100 Oe and 10 kOe field respectively. Each measurement was performed under zero-field cooling (ZFC) and field cooling (FC) respectively. Steep change of $M(T)$ at 327 K could be observed in all the curves, suggesting the establishment of a long-range magnetic ordering at $T = 327$ K. The ZFC data measured under 10 kOe is the same with the FC data. Since high magnetic field may make the spins polarized, the intrinsic magnetic properties of the system may not be completely revealed. Therefore, a small field 100 Oe ZFC is used, which may reflect more intrinsic information of the system. Looking at the ZFC $M(T)$ curve under 100 Oe, we can see that the magnetization keeps a small constant value until 250 K, and increases to the maximum at about 280 K. It drops abruptly at about 327 K and decreases weakly with T increasing further. Such a ZFC $M(T)$ is the typical behavior of the ferrimagnetic ordering or the canted AFM ordering with small net moments. From the data measured at 5 K shown in Fig. 3(c), we get the magnetization to be 1200 emu mol^{-1} at the largest field 50 kOe, equaling to

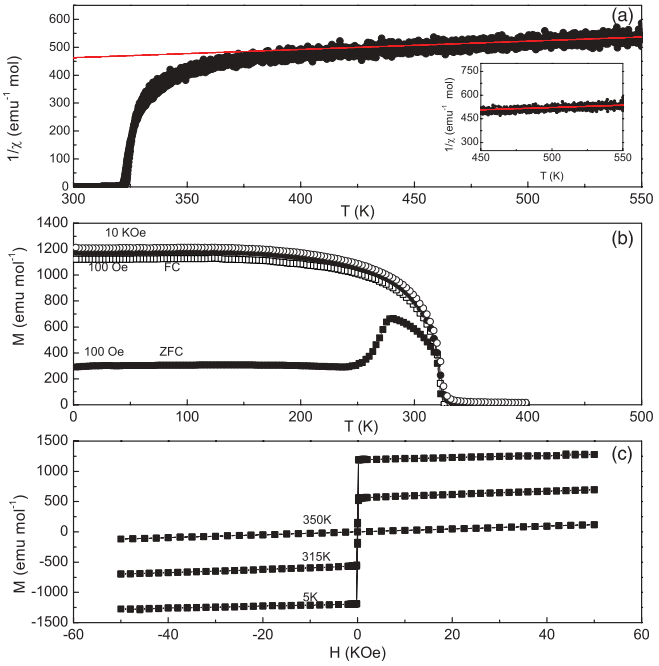

FIG. 3. (Color online) (a) The inverse susceptibility as a function of temperature of the polycrystal $Ca_2Os_2O_7$ between 300 K and 550 K in the field of 10 KOe. The inset is $1/\chi(T)$ from 450 K to 550 K with a red line representing the Curie-Weiss law fitting. (b) The temperature dependencies of the magnetization of $Ca_2Os_2O_7$ single crystal in the magnetic fields of 100 Oe (squares) and 10 KOe (circles) after zero-field cooling (ZFC) (solid ones) and field cooling (FC) (hollow ones), respectively. (c) The field dependencies of the magnetization of $Ca_2Os_2O_7$ measured at 350 K, 315 K, and 5 K respectively.

0.107 μ_B per Os. The net moment is only 3.6% of the expected moment for $S = 3/2$.

In Fig. 4, we plot C_p vs T for single crystal (represented by black squares) and polycrystal (represented by the red circles). The experimental curves of polycrystal and single crystal have the same shape and show phase transition at the same temperature. For both samples, the specific-heat anomaly starts at about 327 K and gets to a maximum at 323 K. It corresponds

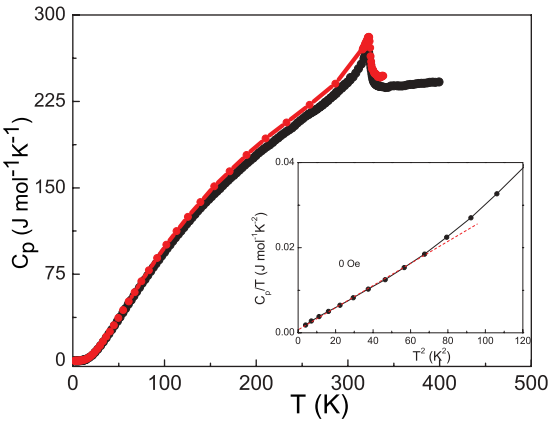

FIG. 4. (Color online) The temperature dependencies of specific heat of ten $Ca_2Os_2O_7$ single crystals (black •) and polycrystals (red •). The inset is the enlargement of the low-temperature part of C_p/T vs T^2.

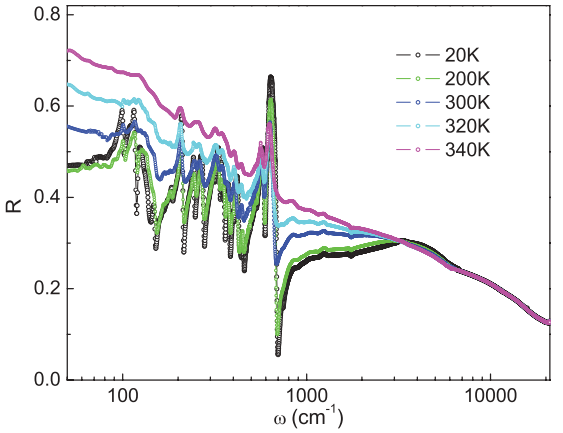

FIG. 5. (Color online) The frequency dependence of reflectivity $R(w)$ at 340 K, 320 K, 300 K, 200 K and 20 K in the frequency region from 50 cm^{-1} to 22 000 cm^{-1}, respectively.

to the transition observed in the resistance and magnetic measurements. The shape of the specific-heat anomaly is λ-like, indicating that the transition is a second-order phase transition. This behavior is consistent with the fact that no crystal structure phase transition was observed in the variable temperature crystal structure analysis in Ref. 9. The inset of Fig. 4 shows the low-temperature part of C_p/T vs T^2 (solid line) and the fitting result (dashed line) using formula $C_p(T)/T = \beta T^2 + \gamma$. One can see that the function could well fit the data at $T < 7$ K. The T^3 term in $C_p(T)$ could be attributed to either phonon or/and magnon contributions. The linear term is the contribution from the electrons. We found that the low-temperature C_p/T approaches a small value (<1.4 mJ mol^{-1} K^{-2}) in the limit of $T \to 0$, indicating the vanishing of the density of states. It implies that the system is fully gapped.

To understand the phase transition, we have to know the electronic structure of $Ca_2Os_2O_7$. Optical spectroscopy is a powerful tool to probe the electronic structure and charge dynamics. We measured the reflectivity spectra from 30 cm^{-1} to 22 000 cm^{-1} at various temperatures and plotted them in Fig. 5. Figure 6 is a collection of the real part of the optical conductivity $\sigma_1(\omega)$ between 20 K and 340 K. The black points in the inset are the dc conductivity from Fig. 2(c), which match with the lowest frequency optical conductivity very well. We can see that there are a lot of phonon responses in the optical conductivity spectra. Even at 340 K, the conductivity decreases with decreasing ω. Although a Drude-like response is not visible, the value of $\sigma_1(\omega)$ at the lowest frequency does not vanish. The data indicate that the compound has a few itinerant carriers at high temperature, which contribute to a small Drude component. A quantitative analysis will be presented below. With decreasing T, the phonon peaks become more pronounced. We found that some modes, for example 577 cm^{-1} and 641.5 cm^{-1}, weakly harden when $T <$ 320 K, indicating some bonds weakly shrinking in the crystal structure.[9]

The conductivity spectra display two interband transition peaks at about 5000 cm^{-1} (about 0.6 eV) and 11 000 cm^{-1} (about 1.3 eV). A full gap could be clearly observed below 200 K. This is also consistent with the zero electron specific

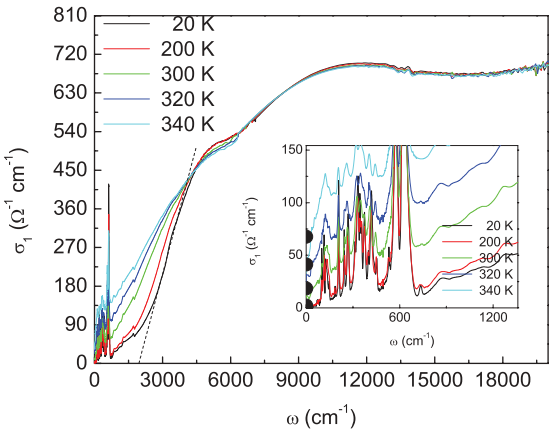

FIG. 6. (Color online) Frequency dependence of the optical conductivity $\sigma_1(\omega)$ at different temperatures. The dashed line shows the steepest dropping of the conductivity and crossing the ω axis, which is defined as the direct gap 2Δ. The inset is the enlarged scale of $\sigma_1(\omega)$ in which the black points are the dc resistivities at the relative temperatures.

heat in Fig. 4. With the temperature decreasing, the spectral weight transfers from low frequency to high frequency and a direct gap opens gradually. To determine the energy gap at 20 K, we draw a dashed line to fit the steepest part of $\sigma_1(\omega)$ in Fig. 6. Extending the line to the ω axis, the crossing appears at $2\Delta \approx 2000$ cm^{-1}, which corresponds to the direct gap. Using the same method, we determine the gap at different temperatures and collect them in Fig. 7, showing how the direct gap develops with the temperature varying. A relatively large gap opens at the same temperature as that shown in the magnetization and specific heat measurements. Consistent with a strongly correlated material, the gap opens at a temperature much lower than the size $k_B T_{\mathrm{AFM}} \ll 2\Delta$.

We noticed that at $T > 300$ K, the optical conductivity spectra do not simply follow the Lorentz line shape in the low-frequency region. As described above, an abruptly increasing reflectivity with the frequency decreasing could be clearly observed in the far infrared region. When the gap completely opens, the reflectivity is almost frequency independent as

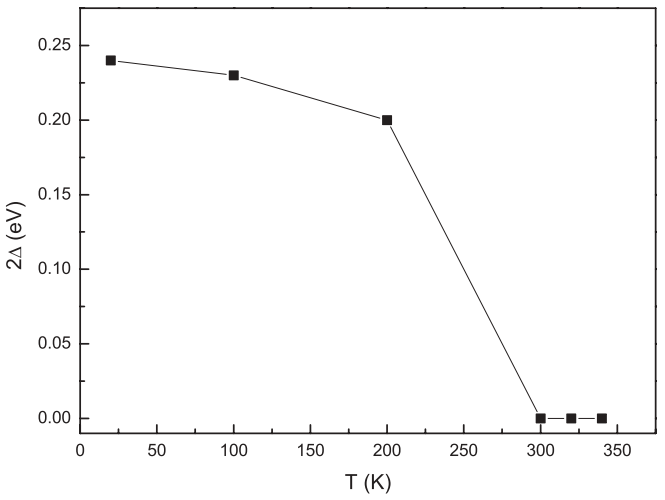

FIG. 7. The development of the direct gap with temperature.

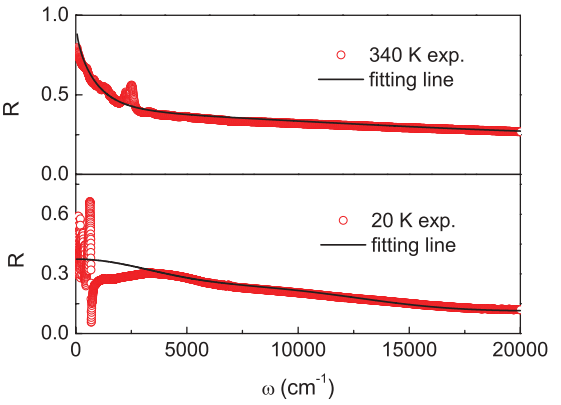

FIG. 8. (Color online) Fitting the frequency dependence of reflectivity $R(w)$ at 340 K and 20 K, respectively. The circles represent the raw data and the solid line is the fitting line using the Drude-Lorentz model.

shown in Fig. 5. We used the Drude-Lorentz model to fit the reflectivity at 340 K and 20 K, respectively,

$$\varepsilon(\omega) = \varepsilon_\infty - \frac{\omega_p^2}{\omega^2 + i\gamma\omega} + \sum_j^N \frac{S_j^2}{\omega_{0j}^2 - \omega^2 - i\gamma_j\omega}, \quad (1)$$

where ε_∞ is the high-frequency dielectric constant; the middle and last terms are the Drude and Lorentz components, respectively. The fitting results are shown in Fig. 8. A Drude term and two Lorentz terms were used to fit the reflectivity at 340 K and 20 K, respectively, which match the raw data very well. The parameters are listed in Table II. This analysis leads to $\omega_p = 4383$ cm^{-1} and the scattering rate $1/\tau = 2572$ cm^{-1} for the Drude component at 340 K. At 20 K, the Drude component becomes vanishing; thus, two Lorentz terms could roughly reproduce the reflectivity as shown in the down-part of Fig. 8. The fitting results confirm that there should be some short-life time itinerant carriers in the system at 340 K, which is completely gapped at 20 K.

III. CALCULATION AND DISCUSSION

The electronic structures of $Ca_2Os_2O_7$ are calculated using density functional method. Because SOC has little influence on the Os^{5+} compounds, we only show the total and projected densities of states (DOS and PDOS) for the nonmagnetic calculation without SOC in Fig. 9. From Fig. 9(a) we can see that the t_{2g} and e_g manifolds are clearly separated from each other due to the octahedral crystal field effect, and from the O $2p$ bands by clean gaps. As a result, the t_{2g} manifolds

TABLE II. The parameters of function (1) at 340 K and 20 K.

T (K)	Function	ω_0(cm^{-1})	ω_p(cm^{-1})	γ(cm^{-1})
340 K	Drude	0	4400	2600
	Lorentz 1	4500	12 600	9300
	Lorentz 2	12 300	22 000	14 900
20 K	Drude	0	0	0
	Lorentz 1	4500	13 600	9300
	Lorentz 2	12 300	22 000	14 900

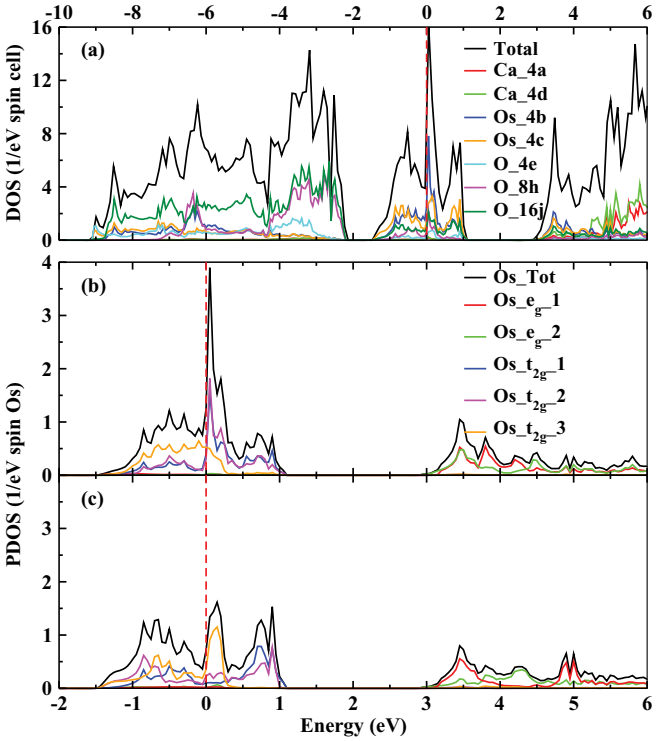

FIG. 9. (Color online) The calculated electronic properties of NM states without SOC. (a) is the DOS and PDOS in a primitive cell. (b) and (c) are the PDOS on 5*d* orbitals of Os(4*b*) and Os(4*c*). Fermi level E_F is defined at 0, denoting as the vertical red dash line.

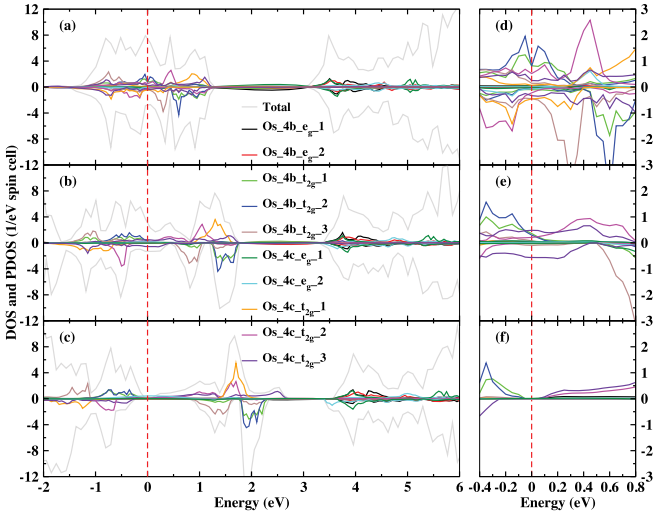

FIG. 10. (Color online) The calculated electronic properties of the collinear AFM states without SOC by GGA ($+U$) method. (a)–(c) are the results calculated by $U = 0$ (GGA), 2, and 4 eV respectively. The positive and negative show partial DOS for up and down spins, respectively. Vertical red dash denotes the Fermi level E_F. (d)–(f) are the enlargements of the Fermi level region of (a)–(c), respectively.

mostly occupy from −1.5 eV to 1.1 eV for both Os 4*b* and 4*c* sites as shown in Figs. 9(b) and 9(c), well separated from the unoccupied e_g manifolds, which are strongly hybridized with O 2*p* orbitals and localized between 3 and 5 eV. We can see that the t_{2g} manifolds are half filled and contain 12 bands, confirming that there are two Os(4*b*) and two Os(4*c*) ions per unit cell, and each Os ion's valence is exactly +5. The t_{2g} band widths for both Os(4*b*) and Os(4*c*) are approximately 2.6 eV, very similar to 2.85 eV of $Cd_2Os_2O_7$,[14] but much wider than Ca_3LiOsO_6's 1.2 eV.[10] This means that: (i) the 4*b* and 4*c* sites have the similar local conditions around Os ions from the nonmagnetic view; (ii) the on-site Coulomb interaction itself could not be responsible for $Ca_2Os_2O_7$'s insulating ground state; (iii) the distance between the nearest Os neighbors $d_{\text{Os-Os}}$ plays an important role for their t_{2g} band width in the Os^{5+} compounds. For example, the average $d_{\text{Os-Os}}$ of $Ca_2Os_2O_7$ is about 3.605 Å, very close to $Cd_2Os_2O_7$'s 3.592 Å, but much smaller than that in Ca_3LiOsO_6 (about 5.648 Å). So that the former two have the similar t_{2g} band widths, while the latter one is much narrower than them.

It should be noted that the high value of DOS at $E_F[N(E_F) = 13.203\ \text{eV}^{-1}$ per cell] obtained in $Ca_2Os_2O_7$ would lead to strong magnetic instability in this material. In order to investigate the possible magnetic order and the insulating ground state, we have performed GGA + U calculation for a collinear AFM state, where the moments on 4*b* and 4*c* sites are assumed to be opposite. The results are shown in Fig. 10, from which we can see that the $N(E_F)$ of GGA is reduced to 7.646 eV^{-1} per cell when collinear AFM is considered, and the total energy is about 155 meV/cell lower than NM state. With U increasing, the up and down spin orbitals on one site will further split, leading to the reduction of $N(E_F)$. An insulating state is reached at $U = 4$ eV. Such a large U is obviously unreasonable for a 5*d* metal oxide. However, if we carefully examine the process of gap opening, some useful clues become clear. One important characteristic of Fig. 10 is that the collinear AFM correlation can obviously narrow the t_{2g} bands on 4*b* sites, while having a weak effect on 4*c* sites. Taking the majority channel (up spin for 4*b* and down spin for 4*c*) calculated by GGA as an example, the band width of 4*b* becomes 2 eV ranging from −1.5 to 0.5 eV, but the band width of 4*c* remains 2.5 eV localized between −1.5 and 1.0 eV. Thus, when the Coulomb repulsion U increases to 2 eV, a full gap opens between up and down spin channels of 4*b* sites as shown in Fig. 10(b), while the 4*c* sites remain metallic until the unreasonable $U = 4$ eV is used. These different behaviors of the electronic structures between 4*b* and 4*c* remind us their different conditions of the nearest-neighbor Os ions. In the view of the nearest Os-Os spin interaction, one 4*b*-site spin is coordinated by four opposite spins on the 4*c* site. However, for the 4*c* site, besides the AFM interaction with four opposite spins on the 4*b* site, it is frustrated with other two 4*c*-site spins (i.e., the spins between 4*c* -sites have ferromagnetic interaction with each other). In this circumstance, we think that the electronic properties of 4*b*-site Os ions in $Ca_2Os_2O_7$ is very similar to NaOsO3,[15] where the gap opening is due to the dual effect of AFM correlation and Coulomb repulsion. On the other hand, the physics on the 4*c* site is more or less like what happened in $Cd_2Os_2O_7$, where magnetic frustration plays an important role. Considering our resistance and optical measurements that $Ca_2Os_2O_7$ undergoes a wide temperature region to transform into the real insulating state, we identify that the electronic structures on the 4*c* site experience a Slater transition.

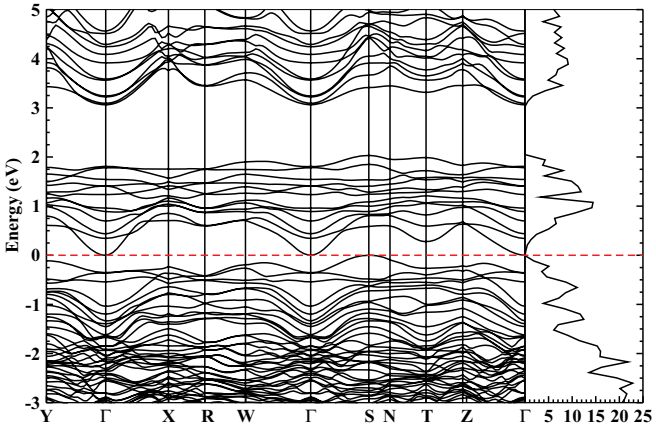

FIG. 11. (Color online) The calculated electronic properties of the noncollinear magnetic states by GGA + U method with SOC and $U = 2.5$ eV. The left panel is the band structure, where the high symmetry points are defined as $Y(0.5,-0.5,0.5)$, $\Gamma(0,0,0)$, $X(-0.377,0.377,0.377)$, $R(0,0,0.5)$, $W(0.25,0.25,0.25)$, $S(0,0.5,0.5)$, $N(0.255,0.378,-0.005)$, $T(0.5,0,0)$, and $Z(0.383, 0.383,-0.383)$, and the right panel is the corresponding DOS with unit 1/(eV cell). Red dash denotes the Fermi level E_F.

In order to find the real magnetic states, magnetic frustration must be correctly dealt with. Thus we perform GGA + U method with SOC to calculate the noncollinear magnetic states of $Ca_2Os_2O_7$, and obtain an insulating solution with a plausible Hubbard U (2.5 eV). The results are shown in Fig. 11, from which we find that a direct gap about 0.35 eV is opened, very close to the data (0.24 eV) deduced by optical measurements. Moreover, based on the noncollinear magnetic DOS, the interband transition at 5000 cm^{-1} (about 0.6 eV) and 12 000 cm^{-1} (about 1.5 eV) in $\sigma_1(\omega)$ correspond to the hopping from −0.2 eV to 0.6 eV and −0.6 eV to 1.0 eV very well. Notes that the Os 5d t_{2g} orbitals are hybridized with O 2p orbitals, and the moments (spin) are noncollinear now, so that the hopping could happen. The calculated moment direction for each Os is shown as an arrow in Fig. 1. We think that the measured net magnetic moments at low temperature are derived from the noncollinear arrangement on Os.

IV. CONCLUSION

We report our specific heat, magnetization, and the optical reflectance investigations on $Ca_2Os_2O_7$. The phase transition is revealed by all the experiments. An energy gap is observed developing with decreasing temperature in the optical measurements. Along with the gap opening, a net ZFC magnetic moment appears and the spectral weight in the low-frequency region is transferred to the higher-frequency region. We performed the first-principles calculations and found that the anti-ferromagnetic (AFM) correlation with intermediate Coulomb repulsion U could effectively split Os(4b) t_{2g} bands and push them away from Fermi level (E_F), while a noncollinear magnetic interaction is needed to push the Os(4c) bands away from E_F, which could be induced by Os(4c)-Os(4c) frustration.

ACKNOWLEDGMENTS

This work is supported by National Science Foundation of China (Grants No. 10834013 and No. 10874213), the 973 project of the Ministry of Science and Technology of China, and Grant-in-Aid for Scientific Research, No. 22246083, from the Japan Society for the Promotion of Science.

[1] A. J. Bosman and C. Crevecoeur, Phys. Rev. **144**, 763 (1966); J. H. de Boer and E. J. W. Verwey, Proc. Phys. Soc. (London) **49**, 59 (1937).

[2] M. Imada, A. Fujimori, and Y. Tokura, Rev. Mod. Phys. **70**, 1039 (1998).

[3] M. M. Qazilbash, A. A. Schafgans, K. S. Burch, S. J. Yun, B. G. Chae, B. J. Kim, H. T. Kim, and D. N. Basov, Phys. Rev. B **77**, 115121 (2008).

[4] N. F. Mott, Proc. Phys. Soc. London, Sect. A **62**, 416 (1949); *Metal-Insulator Transitions* (Taylor and Francis, London, 1990).

[5] P. A. Cox, R. G. Egdellt, J. B. Goodenough, A. Hamnett, and C. C. Naishj, J. Phys. C **16**, 6221 (1983).

[6] B. J. Kim, Hosub Jin, S. J. Moon, J.-Y. Kim, B.-G. Park, C. S. Leem, Jaejun Yu, T. W. Noh, C. Kim, S.-J. Oh, J.-H. Park, V. Durairaj, G. Cao, and E. Rotenberg, Phys. Rev. Lett. **101**, 076402 (2008); B. J. Kim, H. Ohsumi, T. Komesu, S. Sakai, T. Morita, H. Takagi, and T. Arima, Science **323**, 1329 (2009).

[7] K. Ishii, I. Jarrige, M. Yoshida, K. Ikeuchi, J. Mizuki, K. Ohashi, T. Takayama, J. Matsuno, and H. Takagi, Phys. Rev. B **83**, 115121 (2011).

[8] W. J. Padilla, D. Mandrus, and D. N. Basov, Phys. Rev. B **66**, 035120 (2002).

[9] J. Reading, C. S. Knee, and M. T. Weller, J. Mater. Chem. **12**, 2376 (2002).

[10] Youguo Shi, Yanfeng Guo, Shan Yu, Masao Arai, Akira Sato, Alexei A. Belik, Kazunari Yamaura, and Eiji Takayama-Muromachi, J. Am. Chem. Soc. **132**, 8474 (2010).

[11] D. Mandrus, J. R. Thompson, R. Gaal, L. Forro, J. C. Bryan, B. C. Chakoumakos, L. M. Woods, B. C. Sales, R. S. Fishman, and V. Keppens, Phys. Rev. B **63**, 195104 (2001).

[12] A. Bergman, L. Nordström, A. B. Klautau, S. Frota-Pessôa, and O. Eriksson, Surf. Sci. **600**, 4838 (2006).

[13] J. P. Perdew, K. Burke, and M. Ernzerhof, Phys. Rev. Lett. **77**, 3865 (1996).

[14] D. J. Singh, P. Blaha, K. Schwarz, and J. O. Sofo, Phys. Rev. B **65**, 155109 (2002).

[15] Y. G. Shi, Y. F. Guo, S. Yu, M. Arai, A. A. Belik, A. Sato, K. Yamaura, E. Takayama-Muromachi, H. F. Tian, H. X. Yang, J. Q. Li, T. Varga, J. F. Mitchell, and S. Okamoto, Phys. Rev. B **80**, 161104 (2009).